Communication

Direct imaging of DNA fibers: the visage of double helix

Francesco Gentile, Manola Moretti, Tania Limongi, Andrea Falqui, Giovanni Bertoni, Alice Scarpellini, Stefania Santoriello, Luca Maragliano, Remo Proietti Zaccaria, and Enzo Di Fabrizio

Nano Lett., **Just Accepted Manuscript** • DOI: 10.1021/nl3039162 • Publication Date (Web): 22 Nov 2012

Direct imaging of DNA fibers: the visage of double helix

Francesco Gentile[1,2], Manola Moretti[1], Tania Limongi[1,3], Andrea Falqui[4], Giovanni Bertoni[4,5], Alice Scarpellini[4], Stefania Santoriello[1], Luca Maragliano[3], Remo Proietti Zaccaria[1], Enzo di Fabrizio[1,2]*

[1]Nanostructures, [3]Neuroscience and Brain Technologies, [4]Nanochemistry Departments, Istituto Italiano di Tecnologia, Via Morego 30, 16163 Genova, Italy;

[2]BIONEM, Bio-Nanotechnology and Engineering for Medicine, Depertment of experimental and clinical medicine, University of Magna Graecia Viale Europa, Germaneto, 88100, Catanzaro, Italy;

[5]IMEM-CNR, Parco Area delle Scienze 37/A, IT 43124 Parma, Italy

ABSTRACT

Direct imaging becomes important when the knowledge at few/single molecule level is requested and where the diffraction doesn't allow to get structural and functional information. Here we report on the direct imaging of double strand (ds) λ-DNA in the A conformation, obtained by combining a novel sample preparation method based on super hydrophobic DNA molecules self aggregation process with Transmission Electron Microscopy (TEM). The experimental breakthrough is the production of robust and highly ordered paired DNA nanofibers that allowed its direct TEM imaging and the double helix structure revealing.

KEYWORDS:

DNA bundles direct imaging, Transmission Electron Microscopy, Superhydrophobic Surface, Nanofabricated Micropillars, Molecular Dynamics Simulations

The determination of the structure of DNA represented a disruptive historical event and revealed its fundamental role in biology and life science.

However, the understanding of DNA was mainly related to its genetic content that, now we know, represents only a small percentage, about 3%, of the whole information content[1].

The role of the non coding content, about 97%, of our overall genetic material, remained elusive up to recent time, where important discovery were made on the relationship between "non coding DNA", micro RNA and the so called "non functional" or "evolutionary relics" genes[2].

New direct methods are now necessary to understand the complex relationships between DNA, proteins, micro RNAs and transcription factors[3].

Traditionally, the use of diffraction in determining the structure of macro molecules is related to sample preparation optimization and to obtaining high quality crystals or fibers. Unfortunately, only in a minority of cases the crystal can be obtained. An appealing alternative would be to have methods and tools allowing direct imaging of the molecule. In this case, the need of having an organized structure to be solved by diffraction methods would not be required. Nevertheless, there is a deeper reason for trying to develop direct imaging methods: functional information is strictly related to the knowledge of specific epigenetic signatures at level of single molecule. This means that we need tools to unveil the interaction, the structure, the state (genetic, epigenetic conditions) and the function of the coding and non coding content of a DNA molecule[4,5]. In this work, we aimed our effort at direct DNA imaging methods.

Transmission Electron Microscopy is a technique that allows imaging with intrinsic spatial resolution at atomic scale. When working with few biomolecules, there are several factors that worsen the final resolution of the obtained images: i) the poor phase (or absorption) contrast of

atomic species constituting the molecule compared to that of the substrate, where the molecule is sitting; ii) the tendency of the molecule to be fast damaged when investigated by a high energy electron beam[6-8]. However, the situation can dramatically be improved if the molecule is suspended and background free. Under these conditions, the background noise is removed and the spatial resolution is primarily dictated by the intrinsic scattering and absorption cross section properties of the molecule itself, the homogeneity and regularity of the molecular aggregate and by the detector features. The backbone of DNA, formed by phosphates and sugars has enough TEM contrast even when few aligned DNA molecules have to be imaged

In previous experiments, we were able to control the deposition of few DNA molecules on Silicon micropatterned device designed to mimic super hydrophobic (SH) surface[9]. Besides, as a consequence of the deposition method, suspended DNA fibers were observed. In the present experiment, modifying the DNA deposition conditions as well as the device structure, thin and stable suspended DNA fibers could be investigated by the TEM high energy electron beam. Details on the design and fabrication of the device are reported in Methods, By an over layer multistep lithography and reactive ion etching process, we created several passing through holes between the pillars constituting the super hydrophobic surface (Fig. SI 1-3), whose function is to allow the free passage of the electron beam during TEM measurements for having a background free imaging. The preparation in view of the TEM imaging was obtained by allowing the water evaporation from the original liquid sample, at room temperature and 50% relative humidity. The super hydrophobic surface was treated in a way that the adhesion force between it and the water was very low (friction coefficient about 0.02) and, during the evaporation, the pinning of the drop was avoided. Under this condition, after the evaporation, DNA molecules could be deposited suspended and well tense between the pillars, and more importantly several DNA

bundles resulted suspended in correspondence of the holes. The suspended DNA bundles have well reproducible diameter, between 8 and 200 nm at our salinity conditions (see Methods). In Figure 1a is reported a Scanning Electron Microscopy (SEM) overview of this superhydrophobic pillared device, in Figures 1b-c a suspended DNA bundle well aligned with the substrate hole and in Figure 1e its low magnification TEM image. In this last picture the suspended DNA, in substrate free configuration, can easily be observed.

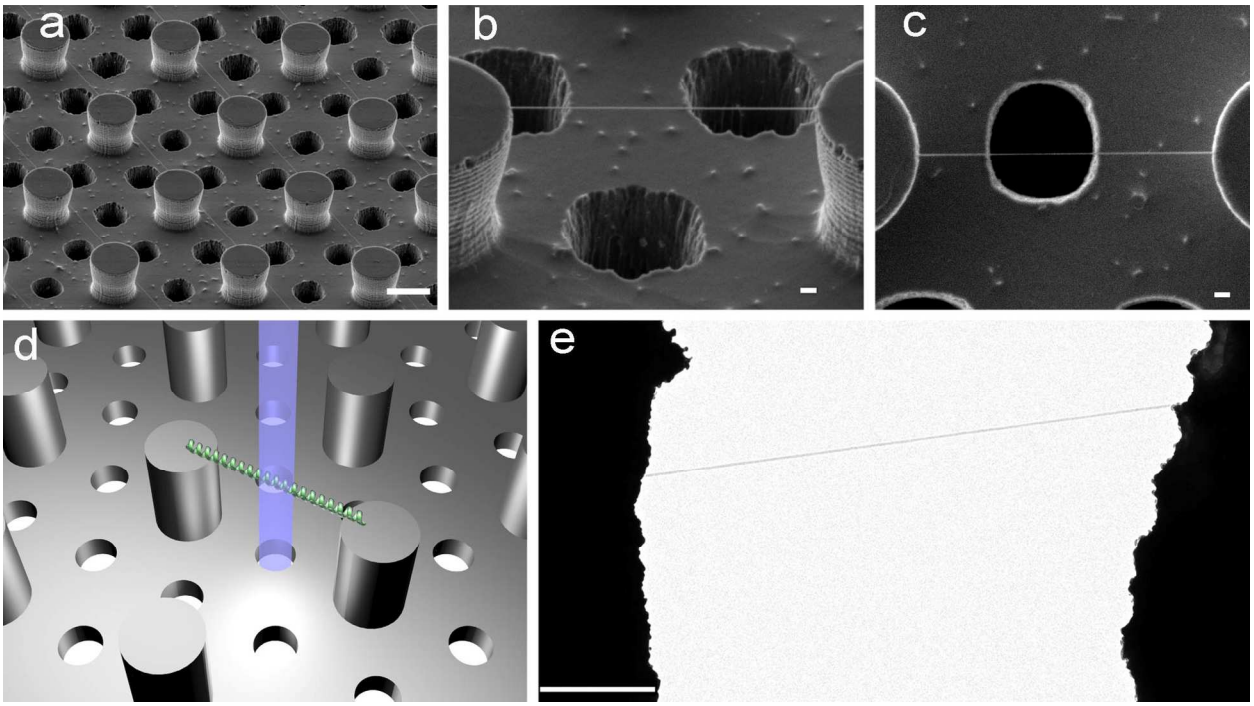

Figure 1. Super hydrophobic DNA molecules self aggregation and TEM use. SEM images (**a**, **b**, **c**), sketch (**d**) and TEM image (**e**) of Lambda DNA suspended on super hydrophobic pillared devices. In detail, an overview of DNA bundles hanging on top of pillars (**a**) and its zoom-in tilted view (**b**) and top view (**c**) showing the DNA bundle located exactly on top of the passing through substrate hole. The sketch (**d**) elucidates the concept exploited for TEM direct imaging: the passing through etched hole allows the suspended DNA to be orthogonally crossed

by the microscope electron beam; *condition sine qua non*: the hole needs to be in line with the pillars in order to allow the DNA bundle alignment. The suspended and aligned DNA bundle is direct imaged through the hole by TEM (**e**). Scale bar in (a) = 10 μm; in (b, c) = 1 μm; in (e) = 500 nm

As shown in the sketch of Figure 1, the suspended DNA corresponding to the hole was brought in front of the electron beam for obtaining direct TEM images. We observed several DNA bundles with different diameter, and in Figure 2 one of the smallest fibers is shown, whose diameter imaged by 100 keV electron beam is about 8 nm, the periodicity is clearly observed. In the inset of the Figure 2a, a magnified portion of the bundle is shown. About 10 periods of DNA can be seen in details. We notice that the period measures 2.7 ± 0.2 nm, corresponding to that known for ds λ-DNA in A conformation. In the panels c of Figure 2, the fiber length measurements of the white selection in b is reported. In panel d, the Fast Fourier Transform (FFT) of the metrological plot is shown, confirming that the dominant spatial frequency is 2.7 nm.

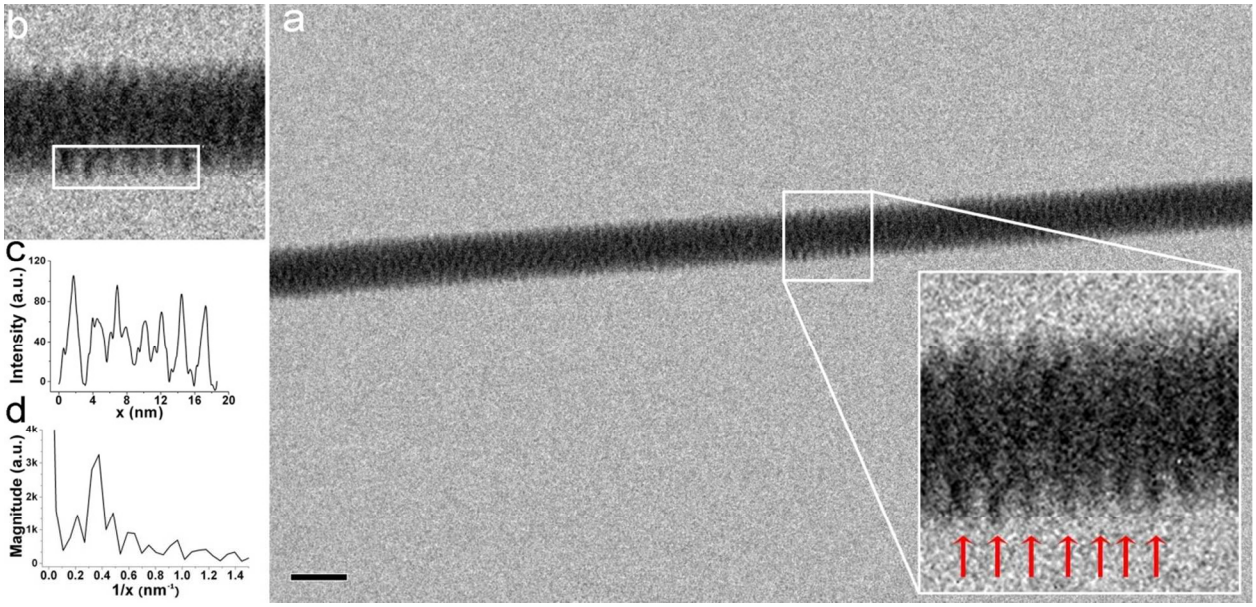

Figure 2. **TEM image with intensity profile and corresponding FFT pitch calculation of λ-DNA fibers**. (**a**) DNA fiber TEM image, the inset shows higher magnification DNA fiber details; the red arrows point out the 2.7 nm pitch of A double helix. The scale bar corresponds to a length of 20 nm. In (**b**) white rectangle is superimposed, showing where the intensity profile was measured. The peaks in the plot **c** correspond to the alternation of bright and dark bands in the original image (**b**), i.e. plot (**c**) displays a two-dimensional graph where the Y-axis reports the pixel intensity integrated along the height of the rectangle and the X-axis represents the distance measured on the rectangle. The plot (**d**) shows the FFT of the signal displayed in plot (**c**): a well defined maximum is observed at 0.37±0.2 1/nm, corresponding to a frequency of 2.7±0.2 nm.

We underline that by this sample preparation the influence of the substrate was completely removed and, in all meaning, the TEM measurement can be then considered substrate free. As a significant consequence, it allowed to get DNA bundles with strong mechanical stability under electron beam up to 300 keV accelerating energy and beam current in the pA range. Besides, due

to their well ordered fiber structure, the structural information of single ds λ-DNA there contained was clearly imaged. All these features permitted to obtain DNA structural details with fundamental metrological precise determination. Two diverse and independent simulations approach allowed to infer that a bundle is formed by paired DNA. This means that ds DNA filaments are aligned with their period along the *z* axis of the helix.

In the first simulation approach we obtained the TEM image of an isolated DNA bundle (background free) by imposing that the smaller bundle whose diameter is equal to 8 nm, is formed by 1+6 ds λ-DNA as shown in Figure 3a (see Methods).

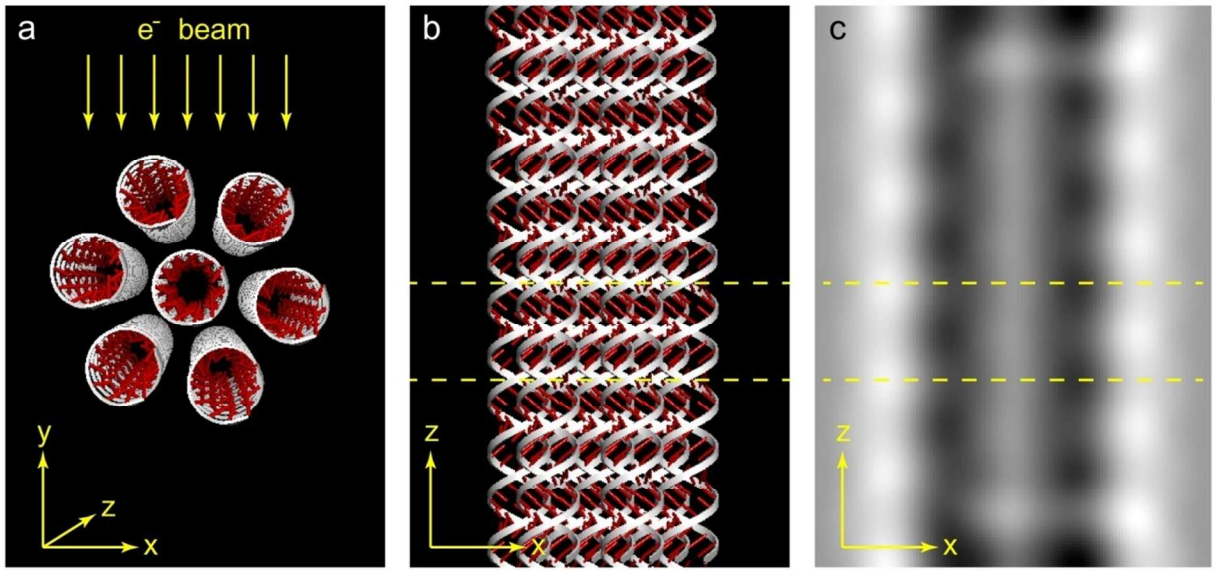

Figure 3. A-DNAs superstructures used for image simulations. (**a**) The smallest bundle consisting in 1+6 A-DNAs (a central one and a shell of 6), the bundle was turned slightly out of low-index zone axis to reduce the contrast in the image due to the coherence created by the superstructure periodicity. The incident parallel electron beam is sketched by the yellow arrows. (**b**) The 1+6 bundle viewed along the y direction and (**c**) the corresponding simulated TEM image at -2 μm defocus with aligned chains.

This bundle structure is in agreement with experimental TEM images (Fig. 2), both in terms of diameter and periodicity. In fact, the 6+1 simulated structure has a bundle diameter very close to that really measured and shown above, and the phase contrast TEM image (Fig. 3c), calculated at the experimental conditions, well reproduces the DNA helix pitch as observed (red arrows in the inset of Fig. 2), measured and reported in Figures 2b-d. Notice that also the experimental and theoretical intensity profile corresponds very well: peaks and minima are shifted by half DNA pitch in the two sides of the bundle. In the Methods section we report the TEM image simulation of more complex bundle structure (Figure SI 4 b), giving details on the relevant parameters used. It is worth notice that if we introduce a random misalignment along *z* axis, larger than 2 base pairs, the periodicity is lost and a blurred image appears in the simulation (Figure SI 5-6).

Figure 4 reports a sketch of the evaporation mechanism on the super hydrophobic surface, where the shear/pulling generated by the radial convection flux and by the drop receding during the evaporation, tend to stretch ds λ-DNA filaments between pillars, as long as the capillary forces, in the perpendicular direction, "push" them to aggregate in bundle during the latest drying phase[10].

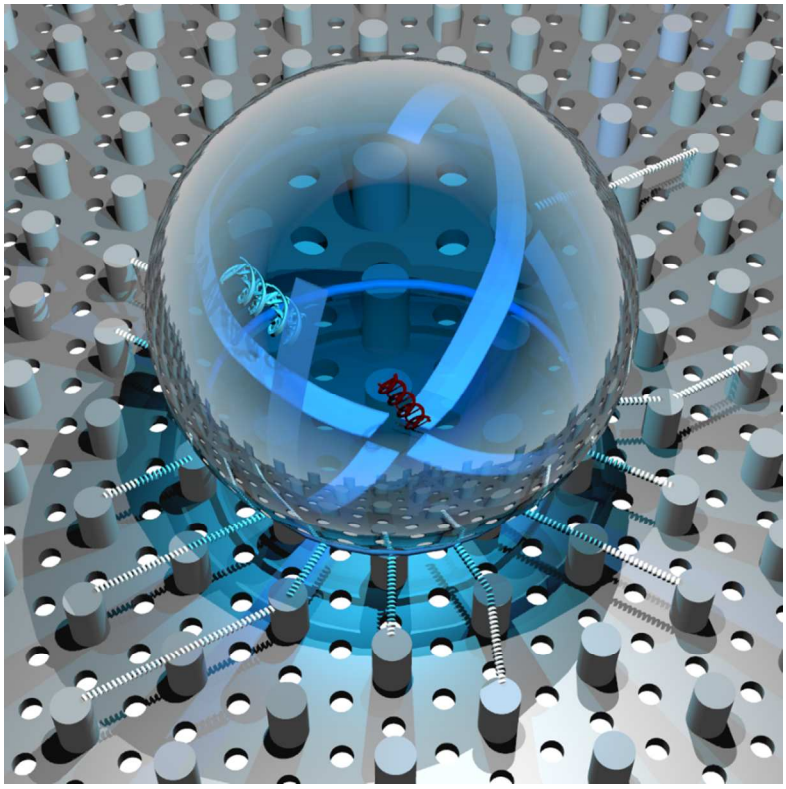

Figure 4. Evaporation and aggregation mechanism. The most practical property of these super hydrophobic surfaces is a reduced friction coefficient (about 0.02 for the present configuration) on account of which they can be conveniently used to deposit, suspend and stretch double strained (ds) lambda DNA molecules between two or more pillars. During the evaporation, the pinning of the drop is avoided, after the evaporation, DNA molecules are suspended and well tense between the pillars and, more importantly, many DNA bundles are in correspondence of the holes. In the aggregation mechanism, capillary forces are responsible for pushing together the ds DNA filaments during the last phase of the evaporation. In particular, shear forces generated by a radial convection flux tend to stretch ds DNA filaments between the pillars, while capillary forces, perpendicular to those shear forces, pack the filaments into aggregates in bundle during the latest drying phase.

In order to further support the model of paired DNA structure, we performed Molecular Dynamics (MD) simulations (see Methods) where we accounted for water evaporation during the bundle aggregation. We started with ds λ-DNA filaments at relative distance of 1 nm and a water volume of 100x100x100 A^3. The ds λ-DNA molecules were left free to move along *z* direction but constrained by a harmonic oscillator potential in direction orthogonal to the same axis. This last choice was suggested by the aggregation mechanism, where capillary forces are responsible for "pushing" together the ds λ-DNA filaments during the last phase of the evaporation.

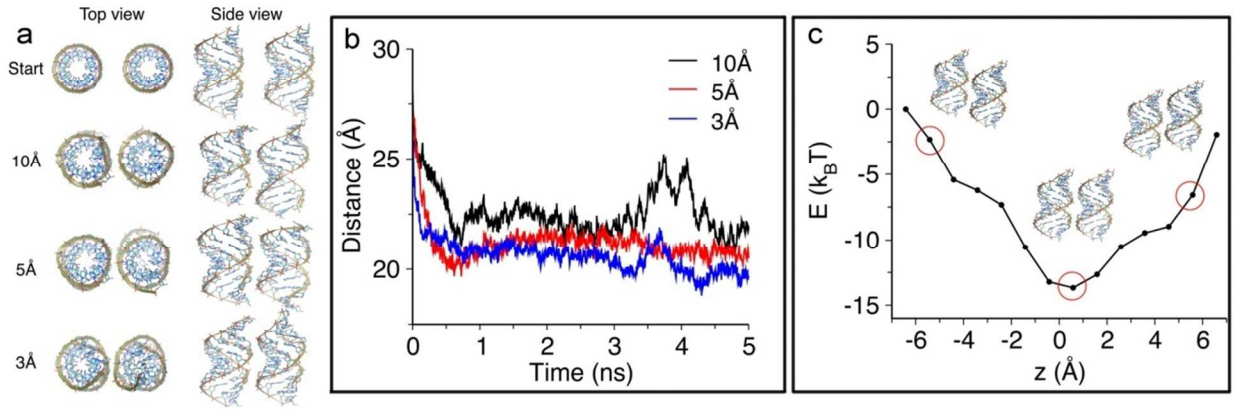

Figure 5 Molecular dynamics simulations of DNA double helices aggregation. (a) Conformations of the paired DNA molecules at the beginning of the simulation and after 5 ns at different hydration conditions; the numbers (A°) refer to the thickness of the hydration layer. (b) Time-evolution of the distance between the centers of mass of the dodecamers along the simulations at different degrees of hydration. (c) Interaction energy (potential of mean force) between the DNA molecules in the 0.3 nm solvation layer as a function of their relative vertical displacement. High and low energy values are highlighted with red circles and the corresponding conformations are shown.

In Figure 5a we report the MD aggregation mechanism and its evolution as a function of starting relative distance between the DNA filaments and a decreasing number of water molecules surrounding the bundle. In Figure 5b the equilibrium separation distance of the double helix filaments is shown, in the starting condition reported in Figure 5a, reached after about 10 ns. The equilibrium distance, center by center, is equal to 2.5 nm and the external backbone distance is 0.3 nm. It is important to remark that also these results well agree with that observed by HRTEM imaging. The whole picture that comes from these results is that both the shear/pulling and the capillary forces, acting as a consequence of the present sample preparation method, are compatible with the inter-helix forces responsible for the DNA pairing. In other words, under the presented superhydrophobic evaporation conditions, the aggregation of ds λ-DNA molecules leads to an ordered fiber structure along *z* axis direction. To further support this view, in Figure 5c we report the calculation of the aggregation free energy as a function of the double helix misalignment in *z* direction. The minimum energy is reached when the alignment condition between the ds λ-DNA filaments is reached with a value, about 12 k_BT, that is big enough for a stable configuration during the latest phase of DNA de-wetting.

We point out at this stage that, incidentally and ironically, our sample preparation route has a strong resemblance with the method used by Wilkins et al.[11] in the historical experimental *tour de force* that brought to DNA structure determination. The pulling and drying fiber preparation by Wilkins et al. was similar to the present method, where the pulling function is played by the convection, and drop receding shear force as well as the drying is played by the evaporation assisted by super hydrophobic surface. The two sample preparation methods lead to similar results, even if the aggregation length scale dominating in our experiment is 3 orders of magnitude smaller than that in Franklin experiment[12]: the fibers obtained by Franklin et al. had a

typical diameter in the range of tens of microns, instead in our case the fiber diameter falls in the range of tens of nanometers. We demonstrated a new preparation method that, based on the use of nanofabricated device, through the evaporation assisted by super hydrophobic self molecular aggregation, allows the DNA fibers HRTEM imaging in background free conditions. For these main reasons, after almost 60 years since the first X-Ray diffraction images[13,14], we were able to obtain, for the first time, a clear direct and completely background-free image of DNA double strand in A conformation by a simple and fast preparation method.

Future developments based on our achievement could be of great interest for genetic and epigenetic analysis, for the understanding on how DNA damage and its repair affect the (epi-) genome over a lifetime, and how these changes impact on age-related pathology and malignant transformation.

Furthermore, there is room for strong further improvements, both in terms of comprehension of the whole mechanism presiding to the DNA bundle formation (a possible supercoiling organization cannot be completely excluded), of sample preparation and TEM analytical perspectives. In the latter case, a new generation of detectors, with increased sensitivity and higher contrast, will permit low dose imaging so that even single DNA helix would resist to high-energy electron beam damage, allowing high quality image detection at single nucleotide level.

Methods

Design and fabrication of the devices. Double polished, (100), 50 μm, p-type thin silicon wafers were purchased from Si-Mat (Silicon Materials, Kaufering, Germany). They were cleaned with acetone and isopropanol to remove possible contaminant and then etched with a 4% wet HF

solution. The wafers were then rinsed with DI water and dried with N_2. A 100 nm layer of chrome was deposited upon the back side of the substrates using a sputter coater (Q150TES Quorum Technologies, Dixon, CA, USA). Standard optical lithography techniques (Suss Microtec MA6/BA6, Sunnyvale, CA, USA) were employed to realize a regular pattern of disks within a layer of positive resist (SPR220), that was spin-coated onto the chrome layer. Therefore, the chrome was removed from the disks by exposing them for 50 s to a standard chrome etching solution (ETCH 18 from OSC-Organo Spezial Chemie, Bitterfeld, Germany). Upon removal of the residual resist with acetone and oxygen plasma, a Deep Reactive Ion Etching (DRIE) process (SI 500 Sentech Instruments Gmbh, Berlin, Germany) was used to etch holes passing through the substrate, the patterned chrome layer serving as a mask. The samples were then immersed in a bath of chrome etching solution to dissolve the remaining chrome. The substrate was then turned upside down, and the fabrication process was pursued on the front side of the samples. A second lithography exposure step was used to realize a regular hexagonal pattern of disks within a layer of negative resist (AZ5214 from Microchemicals GmbH, Ulm, Germany. The discs were positioned exactly on the middle point of each subset of 6 holes. A DRIE process was therefore used, whereby the final pillars were obtained with a height h of about 12 μm, a diameter d of 10 μm and a pitch δ of 30 μm. Further details on SH Device fabrication are reported in Supporting Information.

DNA sample preparation, spotting and Electron Microscopy characterization. Linearized double stranded DNA extracted from Lambda phage (New England Biolabs Inc, Ipswich, MA, USA) was diluted in PBS 1x (containing 0.137 M NaCl) to a final concentration of 50 ng/μl. A 20 μl droplet was post upon the superhydrophobic substrate and let dehydrate overnight at 24 °C and 50% humidity in a petri dish. Samples were then checked without further preparation by

SEM, using a JEOL JSM-7500FA microscope equipped with a cold field emission gun and working at an acceleration voltage of 5 kV The SEM imaging was carried out using the secondary electron signal. Double stranded DNA could be suspended between two pillars during dewetting of a DNA containing droplet on a SH surface as recently shown in Ref. 9 where SH surfaces have been used to concentrate solutes and to precisely deliver few molecules on detection spots. The dewetting droplet is depinning from the pillars posts until a pinning condition due to nanostructure of substrate/drop contact angle[9], high solute, chemical heterogeneicity or discontinuities on the surface are reached[15]. DNA combing is a well-studied method for stretching and aligning nucleotide molecules on flat surfaces or on nanofabricated surface, relying on a flat receding meniscus of solution to stretch the DNA. It could be obtained by pulling out the substrate from the DNA solution (similar to Langmuir-Blodgett preparation) with controlled velocity or by pulling up or sliding a flat surface upon the DNA solution droplet posted on the substrate. Shear flow[16] and exclusion of water molecules[17] at the receding meniscus perpendicular to the droplet evaporation direction are likely contributing to the stretching and alignment of DNA among the pillars. The DNA bundles were finally imaged by TEM with a JEOL JEM-1011 (spherical aberration 5.6 mm), equipped with a W thermionic gun. It operated at an acceleration voltage of 100 kV, and electrons density of 500 $e^-/(Å^2 s)$. The TEM images were collected by a Gatan SC-1000 Orius Camera, equipped with a fiber-optical coupled 11 Mp CCD, and using an acquisition time of 2 s.

TEM Image simulation. The A-DNA superstructures were built using Discovery Studio v3.1 (Accelrys Software Inc.). To avoid boundary effects, approximately 70 bases long nucleic acid chains were built. The DNAs were placed at a 2.5 nm center to center distances, aligned along their axes in a hexagonal pattern, with ideally the same orientation. The TEM image simulations

were performed by using the xHREM v3.5 package (HREM Research Inc.), according to the "multislice method"[18], in which the bundle was divided in 10 phase grating planes of atoms, at which the incident front wave of electrons is dynamically scattered and propagated. The image is calculated taking into account the additional phase and amplitude effects due to the instrument (defocus and aberrations). The choice of a defocus (about -1μm) of the images acquired at the transmission microscopes boosts the low frequencies in the images, permitting to resolve the period of A-DNA (around 2.8 nm), while is cutting the high frequencies, so loosing the information on the bases positions, but with the advantage of cutting noise, that will otherwise affect the in-focus images at such low dose and low contrast due to the low atomic potentials of the constituent atoms. Further details on TEM image simulations are reported in Supporting Information.

Molecular Dynamics (MD) simulations MD simulations were performed using the program NAMD[19] and the CHARMM27[20] force field for DNA molecules. Two filaments of sequence $d(GCGAAATTTGCG)_2$ in A conformation were immersed in a box of 12,331 equilibrated TIP3P[21] water molecules together with 76 Na^+ and 32 Cl^- atoms, which amounts to a 0.137 M/l solution plus excess sodium ions to neutralize the system. The dodecamers were aligned along the *z*-axis, placed at a relative center-to-center distance of about 2.8 nm and zero relative vertical displacement. The full system was simulated with DNA molecules fixed for 10 ns using periodic boundary conditions (PBC), constant temperature (298 K) and constant pressure (1 atm). Electrostatic interactions were computed with the particle-mesh Ewald method[22]. Temperature and pressure were kept constant using Langevin dynamics and the Langevin Nosé-Hoover method[23] as implemented in NAMD. After the cloud of ions equilibrated around the fixed DNA molecules we built different systems at different degrees of hydration by isolating from the full

system the dodecamers, the water molecules and the sodium atoms included in shells of 1, 0.5 and 0.3 nm from the DNAs. The resulting systems were simulated for 5 ns without PBC and using a 10 nm cutoff for electrostatic interactions. The orientation of the dodecamers along *z* was kept fixed by a restraint potential. The free energy for the vertical displacement of the dodecamers was computed for the system with solvation shell 0.3 nm by integrating the mean forces calculated along 14 different restrained simulations, each with the filaments held at different relative displacement by harmonic potentials[24]. The DNA molecules were maintained in the A conformation using a restraint on their root mean square deviation. Each restrained simulation lasted 1 ns to obtain convergence of the mean force estimator.

ASSOCIATED CONTENT

Supporting Information. Additional information on design and fabrication of SH devices and TEM image simulations. This material is available free of charge via the Internet at http://pubs.acs.org."

AUTHOR INFORMATION

Corresponding Author: enzo.difabrizio@iit.it

Author Contributions

E.D.F., F.G. and M.M. conceived and designed the experiments, F.G. and S.S. realized the superhydrophobic devices, M.M., A.F. and A.S. performed the experiments and the EM imaging.

G.B. and L.M. performed the Transmission Electron Microscopy image simulation and the Molecular Dynamics simulations, respectively. E.D.F, A.F., T.L. and R.P.Z. analyzed the data and participated to the writing of the paper. All authors discussed the results and commented on the manuscript.

ACKNOWLEDGMENT

This work was funded under European Project SMD FP7-NMP 2800-SMALL-2 proposal no. CP-FP 229375-2 and under the Single Molecule Activation and Computing (FOCUS) project (Grant agreement no: 270483) funded under 7th Framework Programme.

REFERENCES

(1) Salmena, L.; Poliseno, L.; Tay, Y.; Kats, L.; Pandolfi, P. P. *Cell* **2011**,146, 353.

(2) Biemont, C.; Vieira, C. *Nature* **2006**, *443*, 521.

(3) ENCODE Project Consortium; Bernstein, B.E.; Birney, E.; Dunham, I.; Green, E. D.; Gunter, C.; Snyder, M. *Nature* **2012**, *489*, 57.

(4) Lister, R.M.; Pelizzola, M.; Dowen, R.H.; Hawkins, R.D.; Hon, G.; Tonti-Filippini, J.S.; Nery, J. R.; Lee, L.; Ye, Z.; Ngo, Q. M.; Edsall, L.; Antosiewicz-Bourget, J.; Stewart, R.; Ruotti, V.; Millar, A.H.; Thomson, J. A.; Ren, B.; Ecker, J.R. *Nature* **2009**, *462*, 315.

(5) Harris, R. A.; Wang, T.; Coarfa, C.; Nagarajan, R. P; Hong, C.; Downey, S. L.; Johnson, B. E.; Fouse, S. D.; Delaney, A.; Zhao, Y.; Olshen, A.; Ballinger, T.; Zhou, X.; Forsberg, K. J.; Gu, J.; Echipare, L.; O'Geen, H.; Lister, R.; Pelizzola, M.; Xi, Y.; Epstein, C.B.; Bernstein, B.E.; Hawkins, R.D.; Ren, B.; Chung, W.Y.; Gu, H.; Bock C.; Gnirke, A.; Zhang, M.Q.; Haussler, D.; Ecker, J.R.; Li, W.; Farnham, P. J.; Waterland, R.A.; Meissner, A.; Marr,a M. A.; Hirst, M.; Milosavljevic, A.; Costello, J. F. *Nat. Biotechnol.* **2010**, *28*, 1097.

(6) Bleloch, A.; Own, C.; Hamalainen, M.; Hershleb, J.; Kemmish, K.; Koene, R.; Stark, H.; Stark, J.; Andregg, M.; Andregg, W. *Microsc. Microanal.* **2011**, *17*, 1274.

(7) Cerf, A.; Alava, T.; Barton, R. A.; Craighead, H. G. *Nano Lett.* **2011**,*11*, 4232.

(8) Bell, D.; Thomas, W.; Murtagh, K.; Glover, W. *Microsc. Microanal.* **2011**, *17*, 1276.

(9) De Angelis, F.; Gentile, F.; Mecarini, F.; Das, G.; Moretti, M.; Candeloro, P.; Coluccio, M. L. Cojoc, G.; Accardo, A.; Liberale, C.; Zaccaria, R. P.; Perozziello, G.; Tirinato, L.; Toma, A.; Cuda, G.; Cingolani R.; Di Fabrizio E. *Nat. Photonics* **2011**, *5*, 683.

(10) Smith, S. B.; Finzi, L.; Bustamante, C. *Science* **1992**, *258*, 1122.

(11) Wilkins, M. H. F.; Gosling, R. G.; Seeds, W. E. *Nature* **1951**, *167*, 759.

(12) Franklin, R. E.; Gosling, R. G. *Acta Crystallogr*. **1953**, *6*, 673.

(13) Wilkins, M. H. F.; Stokes, A. R.; Wilson, H. R. *Nature* **1953**, *171*, 738.

(14) Watson, J. D. & Crick, F. H. *Nature* **1953**, *171*, 737.

(15) Deegan, R. D.; Bakajin, O.; Dupont, T. F.; Huber, G.; Nagel, S. R.; Witten, T. A. *Phys. Rev. E* **2000**, *62*, 756.

(16) Accardo, A.; Gentile, F.; Mecarini, F.; De Angelis, F.; Burghammer, M.; Di Fabrizio, E.; Riekel C. *Langmuir* **2010**, *26*, 15057.

(17) Deegan, R. D.; Bakajin, O.; Dupont, T. F.; Huber, G.; Nagl, S. R.; Witten, T. A. *Nature* **1997**, *389*, 827.

(18) Kirkland, E. J. *Advanced Computing in Electron Microscopy*. Plenum, New York, 1998.

(19) Phillips, J. C.; Braun, R.; Wang, W.; Gumbart, J,; Tajkhorshid, E.; Villa, E.; Chipot, C.; Skeel, R. D.; Kalé, L.; Schulten, K. J. *Comput. Chem.* **2005**, *26*, 1781.

(20) Mackerell, A. D.; Feig, M.; Brooks, C. L. J. *Comput. Chem*. **2004**, *25*, 1400.

(21) Jorgensen, W. L.; Chandrasekhar, J.; Madura, J. D.; Impey, R. W.; Klein, M. L. *J. Chem. Phys*. **1983**, *79*, 926.

(22) Darden, T.; York, D.; Pedersen, L. *J. Chem. Phys.* **1993**, *98*, 10089.

(23) Martyna, G. J.; Tobias, D. J.; Klein, M. L. *J. Chem. Phys* **1994**, *101*, 4177.

(24) Maragliano, L.; Fischer, A.; Vanden-Eijnden, E.; Ciccotti, G. *J. Chem. Phys.* **2006**, *125*, 024106.

Graphical Table of Contents (TOC)